Heliyon 10 (2024) e38177

Contents lists available at ScienceDirect

Heliyon

journal homepage: www.cell.com/heliyon

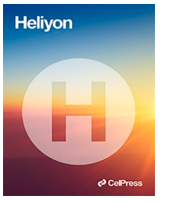

Research article

Multifunctional nitrogen-sulfur codoped carbon quantum dots: Determining reduced glutathione, broad-spectrum antibacterial activity, and cell imaging

Zhipeng Ruan [a,c], Zhifeng Xu [b], Tianhui Liu [a,c], Liwen Chen [a], Xiaoling Liu [a], Kaiying Chen [d], Chengfei Zhao [a,c,*]

[a] Department of Pharmacy, School of Pharmacy and Medical Technology, Putian University, Putian, 351100, China
[b] Department of Cardiothoracic Surgery, Affiliated Hospital of Putian University, Putian University, Putian, 351100, China
[c] Key Laboratory of Pharmaceutical Analysis and Laboratory Medicine (Putian University), Fujian Province University, Putian, 351100, China
[d] Pathology Department, The First Hospital of Putian City, Putian, 351100, China

ARTICLE INFO

Keywords:
Antibacterial activity
Biocompatibility
Carbon quantum dots
Cell imaging
Fluorescence sensing
Reduced glutathione

ABSTRACT

In this study, nitrogen-sulfur codoped carbon quantum dots (N-S/CQDs) with various functions and properties were synthesized through a one-step method utilizing citric acid and cysteine as reaction substrates. The fluorescence of N-S/CQDs can be specifically quenched by permanganate ion (MnO_4^-), and the quenched fluorescence can be recovered by the presence of reduced glutathione (GSH). A fluorescence sensing system based on N-S/CQDs@MnO_4^- was developed and successfully applied for the determination of GSH in pharmaceutical preparations. Additionally, N-S/CQDs demonstrated broad-spectrum antibacterial activity, with minimum inhibitory concentrations of 32 μg/ml against *Staphylococcus aureus* (gram-positive bacterium) and 64 μg/ml against *Escherichia coli* (gram-negative bacterium). N-S/CQDs also proved effective for cell imaging, exhibiting excellent biocompatibility. These findings underscore the multifunctional characteristics and promising application potential of N-S/CQDs. Furthermore, this study provides a solid foundation for the development of multifunctional carbon quantum dots and the expansion of their applications in various fields.

1. Introduction

The unique properties of carbon nanomaterials including carbon nanotubes, graphene sheets and carbon quantum dots, have received more and more attention for their potential applications in biology and medicine [1]. As a kind of new member of carbon nanomaterials, carbon quantum dots (CQDs) with photoluminescent property greatly arouse extensive research for its potential application. Because of unique and superior performance of CQDs, such as low toxicity, biocompatibility, low cost, easy functionalization and chemical inertness, CQDs become the benign substitutes of semiconductor quantum dots containing heavy metals and the star material in research field of life sciences [2,3]. Inspired by the superior advantages of CQDs, extensive research has concentrated on refining simple synthetic methods, enhancing photoluminescence properties, exploring antibacterial activity, and conducting

* Corresponding author. Department of Pharmacy, School of Pharmacy and Medical Technology, Putian University, 1133 Xueyuan Road, Chengxiang District, Putian, 351100, China.
E-mail address: zhaochengfei209@163.com (C. Zhao).

https://doi.org/10.1016/j.heliyon.2024.e38177
Received 11 July 2024; Received in revised form 8 September 2024; Accepted 19 September 2024
Available online 20 September 2024

comprehensive studies of cell imaging.

Several synthetic strategies including acidic oxidation [4], electrochemical carbonization [5,6], laser ablation [7,8], microwave/ultrasonic irradiation [9,10], hydrothermal treatment [11,12], and pyrolysis carbonization [13,14], have been proposed to prepare CQDs in recent years. And many inexpensive and biocompatible starting materials such as sodium citrate [15], glucosamine [16], gelatin [17] ascorbic acid [18], watermelon peels [19], sugar cane juice [20], chitosan [12], and chicken eggs [21], were used as the precursors. And with the rapid development of the CQDs research, a variety of elements doping in CQDs have become a dramatic research interests in application, especially bio-medical field. At present, many nitrogen-doped CQDs were developed and used for the detection of numerous compounds and metal ions, such as glutathione [22], Hg^{2+} [23], Fe^{3+} [24], Cu^{2+} [25], glucose [26], 2,4,6-trinitrophenol [27], and so on.

CQDs have emerged as promising antibacterial agents, demonstrating a range of activities that can be tailored through the choice of precursor materials and synthetic approaches [28]. The exploration of specific bacterial interactions has led to the synthesis of CQDs that exhibit selective antibacterial activity, further enhancing their applicability in biomedical fields [29,30]. Studies have shown that CQDs could effectively inhibit the growth of various bacterial strains, making them useful in antibacterial coatings and wound healing applications [31]. Doping CQDs with heteroatoms like nitrogen, phosphorus, sulfur, or metals significantly enhances their electronic properties and biological activity, notably improving interactions with bacterial cells through mechanisms such as increased photoluminescence and reactive oxygen species generation [32–34].

CQDs are an exciting area of research in the field of cell imaging due to their unique optical properties [35–37]. These nanoparticles, typically less than 10 nm in size, are known for their excellent photostability, biocompatibility, and low toxicity, making them ideal for biological applications [38]. CQDs are characterized by bright luminescence and easily tunable emission wavelengths, making them highly effective for cellular and tissue imaging in various experimental settings [39,40]. These properties stem from their unique surface states and fluorescence capabilities, which allow for vivid imaging across different biological contexts [41]. The ability of CQDs to be doped with various elements also allows for the enhancement of their optical and electronic properties, thereby improving their imaging capabilities in biological tissues [42,43].

In despite of many impressive advances in the synthesis of CQDs, it is still desirous and necessary to rapidly synthesize high-quality CQDs via an easy and environmental method with low-cost raw materials. As we all know, one-step method is considered to be one of the simplest and most cost-effective methods, due to its cheap apparatus, simple manipulation, low energy consumption and good selectivity. Therefore, according to the experience of the previous studies about CQDs, we successfully synthesized nitrogen-sulfur codoped CQDs (N-S/CQDs) with citric acid and cysteine as raw materials.

In this study, we extensively investigated the fluorescence quenching properties of N-S/CQDs in the presence of various ions, as well as the remarkable fluorescence recovery observed after quenching. Additionally, we explored the unique antibacterial activity of N-S/CQDs, highlighting their potential as antimicrobial agents. The study also delved into the cell imaging capabilities of N-S/CQDs, demonstrating their suitability for biological imaging applications. Our findings contribute significantly to the understanding of the optical properties of N-S/CQDs and underscore their multifunctionality, particularly in the fields of biosensing, bioimaging, and antibacterial therapy.

2. Materials and methods

2.1. Chemical reagent

Barium chloride ($BaCl_2$), cupric sulfate ($CuSO_4$), lead acetate ($Pb(CH_3COO)_2$), aluminum chloride ($AlCl_3$), calcium chloride ($CaCl_2$), strontium nitrate ($Sr(NO_3)_2$), zinc sulfate ($ZnSO_4$), magnesium sulfate ($MgSO_4$), ferric chloride ($FeCl_3$), disodium hydrogen phosphate dodecahydrate ($Na_2HPO_4{\bullet}12H_2O$), sodium dihydrogen phosphate dihydrate ($NaH_2PO_4{\bullet}2H_2O$), phosphoric acid (H_3PO_4), sodium hydroxide (NaOH), citric acid and ethylenediamine were purchased from Sinopharm Chemical Reagent Co. Ltd (China). Glutathione (GSH), ascorbic acid, dopamine, glucose, oxidized glutathione, histidine, proline, cysteine, valine, glutamine, phenylalanine, glycine, serine, lysine, aspartic acid, isoleucine, methionine, tyrosine, glutamic acid and cadmium acetate ($Cd(CH_3COO)_2$) were purchased from Sigma-Aldrich Chemical Co. (USA). All other reagents were analytical reagent without further purification. Reduced glutathione tablets (Atomolam) and reduced glutathione for injections (Atomolam) were purchased from Yaopharma Co., Ltd (China). Dialysis membranes (2000) were purchased from Shanghai Yuanye Biological Technology Co., Ltd (China). Ultrapure water obtained from a Millipore water purification system was used in all experiments. *Staphylococcus aureus* (*S. aureus*) (ATCC6538) and *Escherichia coli* (*E. coli*) (ATCC25922) were purchased from Shanghai Luwei Microbial Sci. & Tech. Co. Ltd (Shanghai, China).

Table 1
The results of detecting GSH in pharmaceutic preparations by the proposed fluorescence sensor.

Pharmaceutic preparation	GSH content	Detected content[a]	Labeled amount (%)	Standard deviation
Reduced glutathione tablets	0.1 g/tablet	0.1025 g/tablet	102.5	0.0433
Reduced glutathione for injection	0.6 g/injection	0.6094 g/injection	101.5	0.0514

[a] The data represented the average value of three independent results.

2.2. Synthesis of N-S/CQDs

According to methods previously described, with specific modifications, we prepared the N-S/CQDs [44,45]. The detailed procedure was as follows: 2.5 g of citric acid was combined with 1.0 g of cysteine in a 5 mL beaker and heated to 180 °C using a heating mantle. Within 5 min, the mixture of citric acid and cysteine liquefied. Concurrently, the liquid's color transitioned from colorless to pale yellow and eventually to brown within 15 min. Subsequently, 100 mL of deionized water was introduced to the mixture while continuously stirring. The solution's pH was then adjusted to 5 using 1 mol/L NaOH. This pH-adjusted solution underwent dialysis with a molecular weight cut-off of 1000 for 48 h. The resulting purified N-S/CQDs stock solution, having a concentration of 25 mg/mL, was preserved in the dark at 4 °C when not in use.

2.3. Bacterial culture and preparation of bacterial suspension

All bacteria used in the study were initially inoculated on blood agar plates using the streak plate method and cultured in biochemical incubators at 37 °C to obtain single colonies. A single colony was then selected using an inoculation loop and transferred into sterile normal saline to prepare the bacterial suspension. The OD_{600} value was measured and adjusted to 0.1 using a UV–visible spectrophotometer, yielding a bacterial suspension with a concentration of 1.5×10^8 CFU/mL. This bacterial suspension, with an OD_{600} value of 0.1, could be used directly or diluted for subsequent experiments.

2.4. In vitro antibacterial activity study of N-S/CQDs [46]

The disk diffusion test was conducted by evenly spreading a bacterial suspension, with a concentration of 1.5×10^8 CFU/mL, onto Mueller-Hinton (MH) agar medium using sterile medical swabs. Disks containing the test substances (N-S/CQDs) were then placed on the medium. The MH agar plates had a diameter of 90 mm, and the center-to-center distance between all disks was maintained at a minimum of 24 mm to ensure accurate results. The plates were incubated at 37 °C for 18 h. Following the incubation period, the diameter of the inhibition zone around each disk was measured to determine the antimicrobial activity. Each disk diffusion test was performed in triplicate to ensure reproducibility and reliability of the results.

The broth dilution test involved preparing thirteen sterile test tubes (12 × 75 mm) arranged in a row and numbered consecutively. Tube No. 1 was filled with 1.6 mL of MH broth, while 1 mL of MH broth was added to each of the remaining tubes. To Tube No. 1, 0.4 mL of N-S/CQDs solution at a concentration of 8 mg/mL was added and mixed thoroughly. Subsequently, 1 mL of the mixture from Tube No. 1 was transferred to Tube No. 2 and mixed well. This serial dilution process continued from Tube No. 2 to Tube No. 9. The final 1 mL from Tube No. 9 was discarded. Tube No. 10, which contained no N-S/CQDs, served as the blank growth control. The concentrations of N-S/CQDs in Tubes No. 1 through No. 9 were 2048, 1024, 512, 256, 128, 64, 32, and 16 μg/mL, respectively. Following this, 1 mL of bacterial suspension (1.5×10^6 CFU/mL) was added to each tube, including the control, resulting in a bacterial concentration of 7.5×10^5 CFU/mL in each tube. Consequently, the final concentrations of N-S/CQDs in Tubes No. 1 through No. 10 were 1024, 512, 256, 128, 64, 32, 16, 8, and 0 μg/mL, respectively. These tubes were then incubated at 37 °C for 20 h. The minimum inhibitory concentration (MIC) of N-S/CQDs for the tested bacteria was determined as the lowest concentration in the tubes that remained clear, indicating no bacterial growth.

2.5. TEM characterization of N-S/CQDs antibacterial activity

To evaluate the antibacterial activity of N-S/CQDs using transmission electron microscopy (TEM), a series of meticulous steps were performed. Initially, a 20 μL bacterial suspension with a concentration of 1.5×10^8 CFU/mL was added to 2480 μL of MH broth. After incubating at 35 °C for 6 h, 500 μL of N-S/CQDs solution at a concentration of 5.12 mg/mL was introduced and the mixture was incubated at 35 °C for an additional 12 h. Following incubation, the broth was centrifuged at 3000 rpm for 30 min. The supernatant was discarded to isolate the bacterial sediment, which was then dispersed in 2 mL of 2.5 % glutaraldehyde solution for fixation. The fixation process involved maintaining the sample at 4 °C for 4 h. Subsequently, the sample was centrifuged again at 3000 rpm for 15 min, and the supernatant was removed. To further fix the sample, 1 mL of 1 % osmium acid solution, dissolved in 0.1 mol/L phosphate-buffered saline (PBS), was added and kept at room temperature for 2 h. The sample was then centrifuged at 3000 rpm for 15 min, and the supernatant was discarded. Dehydration was carried out sequentially with ethanol concentrations of 50 %, 70 %, 80 %, 90 %, 95 %, and 100 %, followed by 100 % acetone, each for 15 min. For embedding, the sample was first permeated with a mixture of acetone and 812 embedding agent at ratios of 1:1 for 4 h and 1:2 for 12 h. This was followed by pure 812 embedding agent for 6 h. The sample was then transferred to an embedding plate, dried in a drying oven at 38 °C for 12 h, and polymerized at 60 °C for 48 h. Ultra-thin sections of 60–80 nm thickness were prepared using an ultra-thin microtome. The sections were subsequently stained with a 2 % uranyl acetate saturated alcohol solution and lead citrate for 15 min each. After drying at room temperature for 12 h, the samples were ready for TEM observation. The resulting images were captured and analyzed to assess the antibacterial activity of the N-S/CQDs.

2.6. In vitro cytotoxicity test of N-S/CQDs

Mouse mononuclear macrophages (RAW264.7) were selected to evaluate the *in vitro* toxicity of N-S/CQDs using the MTT assay. A 300 μL cell suspension (2×10^4 cells/mL) was added into 96-well plates to achieve approximately 6000 cells per well. After incubation at 37 °C for 24 h, the cells adhered to the well walls, and the culture medium was discarded. Subsequently, 300 μL of culture medium

containing varying concentrations of N-S/CQDs (32, 64, 128, 256, 512, and 1024 μg/mL) were added to the designated wells. After further incubation at 37 °C for 6, 12, 24, and 48 h, the culture medium was again discarded. Then, 30 μL of 0.5 % MTT solution and 70 μL of serum-free culture medium were added to each well, followed by incubation at 37 °C for 4 h. After incubation, the MTT solution was discarded, and 300 μL of DMSO was added to each well. The plates were then shaken at a low speed for 15 min using an oscillator. The absorbance of each well was measured at a wavelength of 490 nm using a microplate reader. The cell survival rate was calculated based on the measured absorbance values.

3. Results and discussions

3.1. Optical properties of N-S/CQDs

CQDs have emerged as prominent carbon nanomaterials in recent years, with a range of potential applications across different scientific domains. Their unique optical properties, primarily stemming from their quantum confinement effects and edge effects, make them particularly suitable for fluorescence sensing applications [47]. This capability is primarily due to the fact that CQDs can exhibit strong photoluminescence, the intensity and wavelength of which can be tuned based on their size, shape, and surface functionalities [1]. When interacting with various analytes, the fluorescence properties of these CQDs can change, thereby offering a means to detect and quantify the presence of those analytes. Therefore, it is very important to study the optical properties of N-S/CQDs.

The fluorescence spectrums of N-S/CQDs were investigated under varying excitation wavelength from 330 to 370 nm. Fig. 1A showed that the fluorescence intensity of N-S/CQDs reached a peak in the emission spectrum at the excitation wavelength of 345 nm. To meticulously investigate the optical properties of N-S/CQDs, both the UV–Vis absorption spectrum and fluorescence spectrum were comprehensively surveyed. Fig. 1B displayed a characteristic absorption peak at 332 nm in the UV–Vis absorption spectrum (curve a), attributable to the typical n-π* transition of the carbonyl group (C=O) [45]. The absorption peak observed at 332 nm corresponded to the fluorescence excitation spectra recorded at 345 nm (Fig. 1B, curve b). Upon excitation at 345 nm, the N-S/CQDs exhibited robust fluorescence emission, peaking at a maximum fluorescence intensity at 418 nm (Fig. 1B, curve c). Moreover, the fluorescence quantum yield of the prepared N-S/CQDs, with an excitation wavelength (λ_{ex}) of 345 nm, was approximately 25.6 %, determined using quinine sulfate as the reference standard.

3.2. Quenching specificity of N-S/CQDs fluorescence by different ions and recovery of fluorescence after quenching

The intriguing phenomenon of fluorescence quenching and subsequent recovery in CQDs provides a potential application framework for the establishment of fluorescence-based sensing systems [48]. Upon the introduction of a specific quenching compound, the innate fluorescence of CQDs is noticeably quenched, marking a preliminary yet crucial step in the analytical process [49]. This quenching effect can be attributed to the interactions between the quenching compound and the CQDs, resulting in a significant reduction in the fluorescence emission [49]. However, this quenching is not a terminal state, and the quenched fluorescence can be notably restored by the addition of a particular restorative compound [50]. This recovery process emphasizes the reversibility of fluorescence quenching, a crucial feature essential for real-time monitoring and detection in analytical applications [50]. The recovery of quenched fluorescence is not only a reversal, but also a vital characteristic that amplifies the versatility and effectiveness of CQDs-based fluorescence sensing systems. This unique characteristic enables a dynamic, responsive, and robust fluorescence sensing paradigm, thereby broadening the horizons for real-time, accurate sensing and detection of various analytes in diverse settings [49]. Furthermore, the interaction between the specific compounds and CQDs, which governs the quenching and recovery of fluorescence, opens up a realm of possibilities in designing tailored sensing systems with enhanced selectivity and sensitivity [51].

The effect of various metal ions on the fluorescence of N-S/CQDs is vividly experimented, including Zn^{2+}, Mg^{2+}, Fe^{2+}, Cu^{2+}, Mn^{2+}, Ca^{2+}, Cd^{2+}, Ag^{+}, Ni^{2+}, Co^{2+}, Fe^{3+}, and MnO_4^-. As shown in Fig. 2A, none of these common metal ions significantly affect the fluorescence intensity of N-S/CQDs. However, MnO_4^- could stand out for its significant quenching effect on the fluorescence of N-S/CQDs by more than 90 % in Fig. 2A, underlining a distinct quenching effect which is a critical aspect in fluorescence studies, often related to

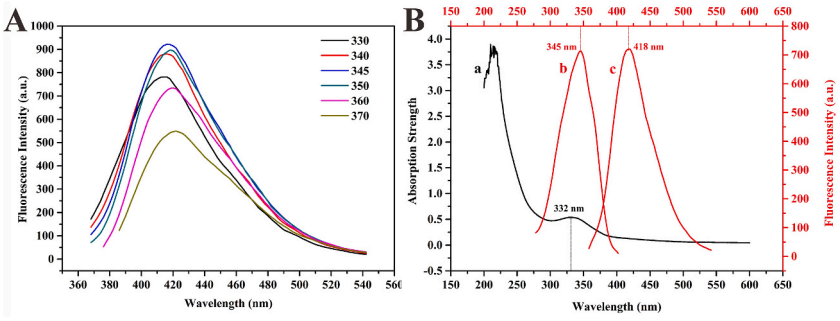

Fig. 1. (A) The emission curves of N-S/CQDs with the different excitation wavelengths; (B) UV–vis absorption spectrum (a), fluorescence excitation (b), and emission (c) spectra of N-S/CQDs.

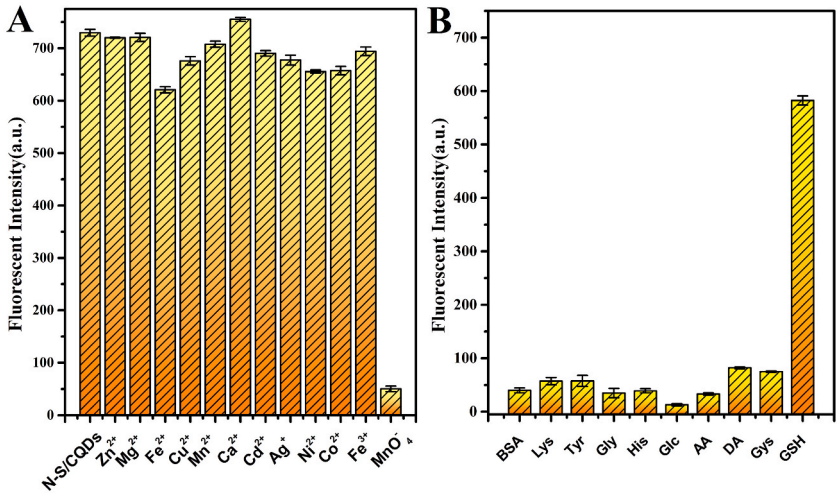

Fig. 2. (A) Quenching effect of different metal ions and MnO_4^- for N-S/CQDs fluorescence. (B) Recovery effect of different compounds for N-S/CQDs fluorescence quenched by MnO_4^-.

the electronic interactions between the fluorophore and quencher. This quenching phenomenon suggests potential pathways for modulating the fluorescence characteristics of the N-S/CQDs, which could be instrumental in developing sensitive detection methods based on MnO_4^-.

When the fluorescence of N-S/CQDs was significantly quenched by MnO_4^-, several compounds were reintroduced, including lysine, tyrosine, glycine, histidine, glucose, ascorbic acid, dopamine, cysteine, and GSH. Notably, among these, GSH was particularly effective in restoring the quenched fluorescence, as depicted in Fig. 2B. This restoration suggests a potential protective mechanism of GSH against the fluorescence quenching of N-S/CQDs, which could be critical for biomedical applications where fluorescence recovery is required. The fluorescence of N-S/CQDs is effectively quenched by MnO_4^-, subsequently restored by the addition of GSH. This phenomenon heralds a significant advancement in the study of fluorescence modulation mechanisms in CQDs, setting a robust foundation for the innovation of novel methodologies for assaying GSH. Furthermore, the exploration of interactions between fluorescence quenchers and restorers not only enriches our understanding of the optical properties of doped CQDs but also unveils potential applications in diverse analytical fields. This research area promises to enhance our ability to control and exploit the fluorescence characteristics of CQDs for various scientific and industrial applications, thereby broadening the scope of their utility.

3.3. Quenching effect of MnO_4^- with different concentration on N-S/CQDs fluorescence

The investigation into the interplay among diverse ions and CQDs has emerged as a subject of intense fascination within the domains of nanotechnology and materials science. This interest largely stems from observations of the quenching effect that occurs when different ions are introduced into the fluorescent milieu of CQDs, highlighting their potential applications in sensing technologies. Extending this research, the study explored the quenching impacts of permanganate ions at varying concentrations on the fluorescence of N-S/CQDs, thereby revealing nuanced insights into their quenching mechanisms and enhancing the prospects for developing advanced sensors.

Shi et al. reported the quenching effects of lead ion (Pb^{2+}) on N-S CQDs fluorescence, where the fluorescence was quenched due to a specific interaction between Pb^{2+} and the carboxyl and sulfhydryl on the surface of the CQDs [52]. Similarly, Wang et al. reported that the fluorescence of N-CQDs was quenched quantitatively by hypochlorite ion (ClO^-) and hexavalent chromium ion (Cr^{6+}), and further verified that the N-CQDs played an excellent role in detecting the two ions of actual water samples [53]. They further confirmed that the quenching mechanism of ClO^- was dominated by static quenching, while the quenching mechanism of Cr^{6+} was mainly due to inner filter effect [53]. Elhaleem et al. reported that the fluorescence of N,S-CQDs was quantitatively quenched upon addition of imatinib (IMA), and was therefore used for the determination of IMA in pharmaceutical preparations and biological fluids [54]. They found that the fluorescence quenching of N,S-CQDs by imatinib was mainly attributed to the mechanism of static quenching [54]. Yang et al. reported that the fluorescence of N,S-GQDs could be quenched by Fe^{3+} and Hg^{2+}, and confirmed that the mechanisms of fluorescence quenching for detecting Fe^{3+} and Hg^{2+} were mainly attributed to the inner filter effect (IFE) and dynamic quenching process, respectively [55].

Based on the convergent findings of multiple studies, it is plausible to hypothesize that the quenching effect observed when MnO_4^- interact with N-S/CQDs is mediated by a consistent underlying mechanism. This hypothesis is supported by the consistent patterns of fluorescence attenuation observed in these studies when MnO_4^- are introduced to the N-S/CQDs system. This interaction likely involves the dynamic quenching of fluorescence through a process such as electron transfer or energy transfer between MnO_4^- and N-S/CQDs. Consequently, elucidating this mechanism can significantly broaden the spectrum of potential applications for sensors that are based on N-S/CQDs and MnO_4^-. Such sensors could be effectively utilized in various detection contexts, including environmental monitoring

and biomedical diagnostics, where sensitive and specific detection of chemical or biological agents is critical. Further research should aim to comprehensively characterize the interaction between N-S/CQDs and MnO_4^- to optimize the design and function of these novel sensors.

Fig. 3 illustrates the quenching phenomenon exhibited by varying concentrations of MnO_4^- on the fluorescence of N-S/CQDs. The graphical representation clearly depicts a trend where the fluorescence intensity of N-S/CQDs diminishes observably as the concentration of MnO_4^- increases from a baseline of 0 mol/L to a substantial concentration of 1000 μmol/L. This trend demonstrates a significant concentration-dependent quenching effect, consistent with Stern-Volmer quenching theory. The diminishing fluorescence intensity underlines a plausible interaction between MnO_4^- and N-S/CQDs, which could be attributed to the electron transfer mechanism, a fundamental mechanism frequently explored in studies of fluorescence quenching. Furthermore, the concentration-dependent relationship between the fluorescence quenching of N-S/CQDs and MnO_4^- demonstrates potential analytical utility, whereby N-S/CQDs may serve as a sensitive fluorescence probe for the detection of MnO_4^- [56]. This aligns with recent advances in the use of CQDs as fluorescent probes for ion detection, a field that has attracted significant scholarly interest because of its importance in environmental monitoring and analytical chemistry [57]. The study illustrated in Fig. 3 contributes significantly to the expanding corpus of knowledge by elucidating the crucial interactions between CQDs and ion concentrations. This enhancement in understanding paves the way for broader applications of CQDs in fluorescence-based sensing technologies.

3.4. Linear relationship between the concentrations of adding GSH and the intensity of fluorescence recovery

In this study conducted under the optimized experimental conditions, a thorough investigation was carried out to elucidate the correlation between the intensity of fluorescence recovery and the amount of adding GSH, as illustrated in Fig. 4. In Fig. 4A, a notable observation was that the fluorescence recovery intensity of N-S/CQDs demonstrated an increasing trend with rising GSH concentrations. This fascinating finding suggests the possibility that GSH, a well-known antioxidant, may interact chemically with MnO_4^- within the orchestrated reaction system. This interaction is critical as it provides fundamental insights into the behavior of the system being investigated. Evidence supporting this phenomenon may be found in various studies validating interactions between reactive substances within frameworks similar to quantum dot.

Fig. 4B further elucidates the relationship by demonstrating a linear correlation between the intensity of fluorescence recovery (denoted as F) and the concentration of adding GSH (denoted as C_{GSH}). The regression equation derived from the linear correlation, $F = 0.4963C_{GSH}\text{-}1.958$, with a coefficient of determination (R^2) of 0.9937, confirms the strong linear relationship between these variables. The depicted linear relationship is reminiscent of the principles of Beer-Lambert Law, which posits a linear correlation between the concentration of an analyte and its absorbance (or in this context, recovered fluorescence). The intrinsic linearity of this relationship is fundamental as it facilitates the simplification of quantification and analysis within the reaction system—a central theme in numerous analytical chemistry studies. The high R^2 value not only reaffirms the linear relationship but also highlights the precision and reliability of the fluorescence method used to quantify GSH concentrations—a technique frequently praised for its sensitivity and accuracy in analytical applications. Through a rigorously defined regression model, this study establishes a robust mathematical framework for the quantitative analysis of the impact of GSH concentration on fluorescence recovery. This is instrumental in advancing the understanding of the reaction system and may potentially pave the way for further investigations into the reactive dynamics of N-S/CQDs across various biochemical environments.

3.5. Detection of GSH in pharmaceutical preparations by the fluorescence sensor based on N-S/CQDs and MnO_4^-

The proposed fluorescence sensor operates on the principle that the fluorescence of N-S/CQDs is quenched by MnO_4^-. However,

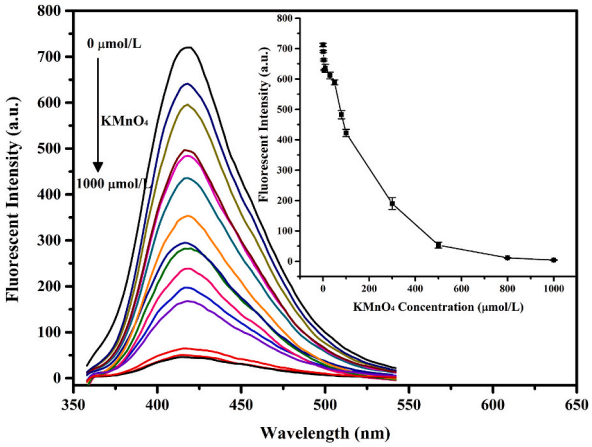

Fig. 3. Fluorescence spectra of N-S/CQDs fluorescence quenching by MnO_4^- with different concentation from 0 to 1000 μmol/L. The inset is a line diagram of the change in N-S/CQDs fluorescence quenching by MnO_4^- with different concentation from 0 to 1000 μmol/L.

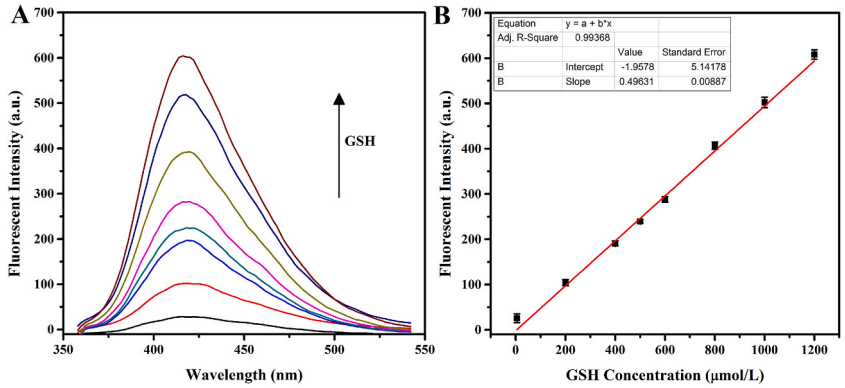

Fig. 4. (A) The restored fluorescence spectra of N-S/CQDs@MnO_4^- by the addition of GSH in the range from 5 to 1200 μmol/L; (B) The linear relation between the intensity of fluorescence recovery of N-S/CQDs@MnO_4^- and the different concentrations of GSH in the range from 5 to 1200 μmol/L.

when GSH is added again, it may react with MnO_4^-, leading to the recovery of the fluorescence signal. The intensity of fluorescence recovery is proportional to the concentration of adding GSH, allowing for its accurate quantification.

In this study, the sensor was used to measure the GSH content in reduced glutathione tablets and reduced glutathione for injection, and the results were shown in Table 1. The results showed that the GSH content per tablet was 0.1025 g in reduced glutathione tablets, and the GSH content per injection was 0.6094 g in reduced glutathione for injection. These two values correspond to labeled amounts of 102.5 % for the tablets and 101.5 % for the injections. These two results are in line with the standards set by the Chinese Pharmacopoeia (2020 Edition), which stipulates that the range of labeled amount for these two pharmaceutical preparations should be between 93 % and 107 %.

The consistency of the results with the pharmacopoeia standards demonstrates the accuracy and reliability of the proposed method. This indicates that the fluorescence sensor based the combination of N-S/CQDs and MnO_4^- can be effectively used for the detection of GSH in pharmaceutical preparations. The high sensitivity and specificity of this sensor make it a valuable tool for quality control in the pharmaceutical industry.

3.6. Linear relationship between the concentrations of adding GSH and the intensity of fluorescence recovery in serum

The investigation of fluorescence sensors within the realm of clinical practice represents a convergence of nanotechnology and biomedical science. This study aimed to evaluate the feasibility of the fluorescence sensor for clinical applications, with a specific focus on measuring GSH levels in serum samples. To this end, a comprehensive assessment was performed using a simulated serum system, which employed serum from healthy volunteers as a surrogate. This approach was intended to determine whether the fluorescence sensors could accurately quantify GSH levels in complex biological matrices, thereby mirroring conditions encountered in actual clinical settings.

The primary objective of this analysis was to establish a linear relationship between the recovered fluorescence intensity (F) and the

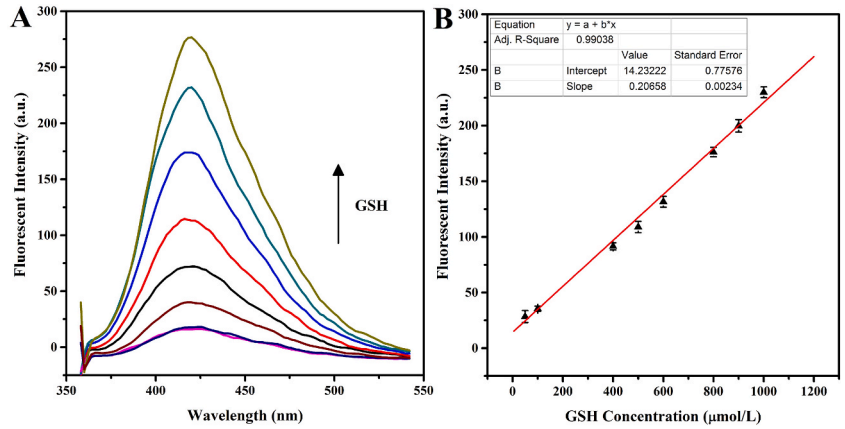

Fig. 5. (A) The restored fluorescence spectra of N-S/CQDs@MnO_4^- by the addition of GSH in the range from 50 to 1000 μmol/L in serum; (B) The linear relation between the intensity of fluorescence recovery of N-S/CQDs@MnO_4^- and the different concentrations of GSH in the range from 50 to 1000 μmol/L in serum.

GSH concentration (C_{GSH}). This relationship is clearly depicted in Fig. 5, which shows a consistent increase in fluorescence intensity with rising concentrations of GSH, thereby confirming a linear correlation between these variables. This relationship is quantitatively described by the regression equation $F = 0.2066C_{GSH}+14.23$, with a coefficient of determination (R^2) of 0.9904, indicating a strong and reliable linear relationship in the simulated serum system. Such linearity is a prerequisite for any analytical tool, as it ensures the ability to deliver precise and reliable measurements across a range of concentrations.

Numerous techniques have been utilized for both the identification and quantification of GSH, including high-performance liquid chromatography (HPLC), electrochemical approaches, and particularly fluorescence spectroscopy [58]. Each technique offers distinct advantages, contributing uniquely to the robust analysis and accurate measurement of GSH in various biological samples. The fluorescence-based detection approach, utilizing the Au@PLL–AEDP–FITC probe-based fluorescence-enhanced "turn-on" strategy, has demonstrated substantial sensitivity, rapidity, and efficacy for the detection of GSH [59]. This method is particularly effective in complex biological environments such as cellular systems, indicating its promising potential for future applications in biomedicine. The utilization of this strategy enhances the detection capabilities in challenging biological matrices, making it a valuable tool for advancing research in cellular and molecular biology.

A specific fluorescent nano-platform was developed exhibiting excellent selectivity and successful application for GSH detection in human serum plasma, which underscores the practicability of fluorescence sensors in biological and clinical applications for GSH sensing [60]. Additionally, a sensitive fluorescence sensor based on MnO_2 nanosheets-copper nanoclusters composites showcased the potential for sensitive detection of glutathione, further broadening the horizons for fluorescence sensor applications in clinical diagnostics [61].

These findings and technological advancements highlight the significant potential of fluorescence sensors in offering straightforward, precise, and real-time detection of GSH in practical serum samples. This capability is particularly promising for clinical practice, as it could lead to improved diagnostic accuracy and more efficient patient management. By leveraging the sensitivity and specificity of these sensors, clinicians may soon be able to detect and monitor GSH levels quickly and effectively, facilitating timely interventions and better health outcomes. Overall, the integration of fluorescence sensors into clinical settings appears to be a promising advancement in medical diagnostics.

3.7. Antibacterial activity of N-S/GQDs

In the realm of antibacterial research, the diversity of carbon sources from which CQDs are derived allows them to exhibit a variety of functional properties, including unique antibacterial capabilities [1,31,62]. Specifically, CQDs derived from gentamicin sulfate not only match the antibacterial activity of the antibiotic but also show potential in disrupting mature biofilms of *S. aureus* without developing resistance [63]. Therefore, in this study, we conducted a detailed study on the antibacterial activity of N-S/CQDs.

The disk-diffusion test, often referred to as the Kirby-Bauer test, is a standardized and widely employed method in clinical microbiology for determining the susceptibility of bacteria to antibiotics. This test is crucial for guiding antibiotic therapy and is commonly utilized in various healthcare settings to assess the effectiveness of antibiotics against bacterial infections. In this study, the antibacterial activity of the prepared N-S/CQDs against *S. aureus* and *E. coli* was evaluated by disk-diffusion test, as shown in Fig. 6A

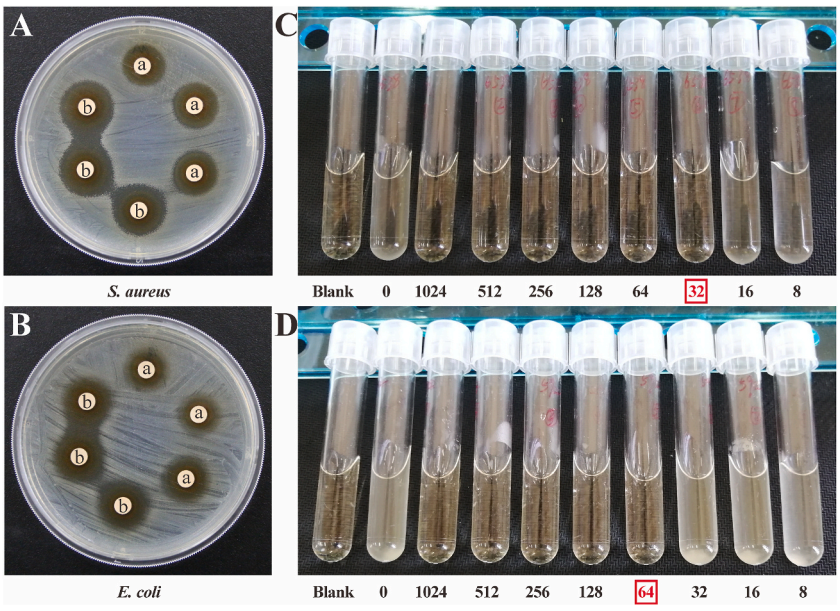

Fig. 6. Antibacterial activity of N-S/CQDs against *S. aureus* (A) and *E. coli* (B) on MH agar plates. Disks a and b contain 0.5 mg and 0.25 mg of NCQDs, respectively. MIC tests of N-S/CQDs against *S. aureus* (C) and *E. coli* (D) on MH broth.

and B. On MHA plates, disk a and disk b contain 0.5 mg and 1.0 mg of prepared N-S/CQDs, respectively. The results showed clear zones of inhibition around the disks impregnated with N-S/CQDs on MHA plates coated with *S. aureus* and *E. coli*, suggesting dose-dependent antibacterial activity and broad-spectrum antibacterial potential.

The broth dilution test is a microbiological method used to determine the MIC of an antimicrobial agent against specific microorganisms. This test is vital for assessing the susceptibility of bacteria, fungi, or other pathogens to various antimicrobial substances. It plays a critical role in guiding the selection of antimicrobials in clinical settings and monitoring trends in antimicrobial resistance. The broth dilution test can be conducted in two formats: macrobroth, which utilizes larger volumes in test tubes, and microbroth, which employs smaller volumes in microtiter plates. In this study, we assessed the MIC of the prepared N-S/CQDs against two prominent bacterial strains: *S. aureus* and *E. coli*. Utilizing the macrobroth dilution method, the MIC values were determined to be 32 μg/mL for *S. aureus* and 64 μg/mL for *E. coli*, respectively, indicating a more potent effect against *S. aureus*, as shown in Fig. 6C and D.

TEM characterization was performed to observe the morphological changes in bacteria before and after treatment with N-S/CQDs, as shown in Fig. 7. Fig. 7A and C presents TEM images of *S. aureus* and *E. coli* cultured under normal conditions, respectively. The bacteria cultured under these conditions displayed normal cell structure, with intact cell walls and uniform intracellular material density. In contrast, Fig. 7B and D depict the morphology of *S. aureus* and *E. coli* after treatment with N-S/CQDs. Significant morphological alterations are evident, including pronounced disruption of the cell wall and membrane, partial disintegration of bacterial cells, and the appearance of cavities and material aggregation within the cells. These changes lead to the loss of bacterial cell integrity, causing irreversible damage and ultimately bacterial death. The observed morphology after N-S/CQDs treatment markedly differs from that under normal conditions and resembles TEM images of bacteria treated with other known antibacterial agents reported in thesr literatures [46,64]. This indicates that N-S/CQDs exert a substantial destructive effect on both gram-positive and gram-negative bacterial cells, demonstrating their potent antibacterial activity.

These findings suggest that N-S/CQDs possess a broad-spectrum antibacterial activity, potentially linked to their size, surface functional groups, and ability to generate reactive oxygen species. Regarding its antibacterial mechanism, the surface properties and size of N-S/CQDs may play a crucial role in its antibacterial effect. Nanoscale N-S/CQDs can penetrate bacterial cells more effectively, causing substantial damage and inhibiting bacterial growth. Additionally, anchoring specific groups on the surface of N-S/CQDs can enhance their interaction with bacterial cell membranes, potentially improving their antimicrobial activity. For instance, by introducing functional groups such as amine groups, CQDs can be given a positive charge which increases their interaction with the negatively charged bacterial cell membranes, leading to improved antibacterial action against both gram-positive and gram-negative bacteria [65]. The antibacterial efficacy of CQDs can be markedly enhanced through further strategic modifications or functionalization, without inducing resistance [66,67]. This suggests that by manipulating the surface characteristics and size of N-S/CQDs, their antibacterial properties can be optimized, opening new avenues for the development of advanced antibacterial materials.

The efficacy of N-S/CQDs against these common pathogens is particularly noteworthy given the rise of antibiotic resistance, positioning N-S/CQDs as a viable candidate for novel antibacterial agent development. Further research could explore the antibacterial mechanisms of N-S/CQDs at the cellular level, optimizing their properties for enhanced antibacterial efficiency. Expanding upon these findings, future studies could explore the application of N-S/CQDs in developing coatings for medical devices, where their antibacterial properties could prevent the formation of biofilms and reduce hospital-acquired infections, presenting a promising avenue for further

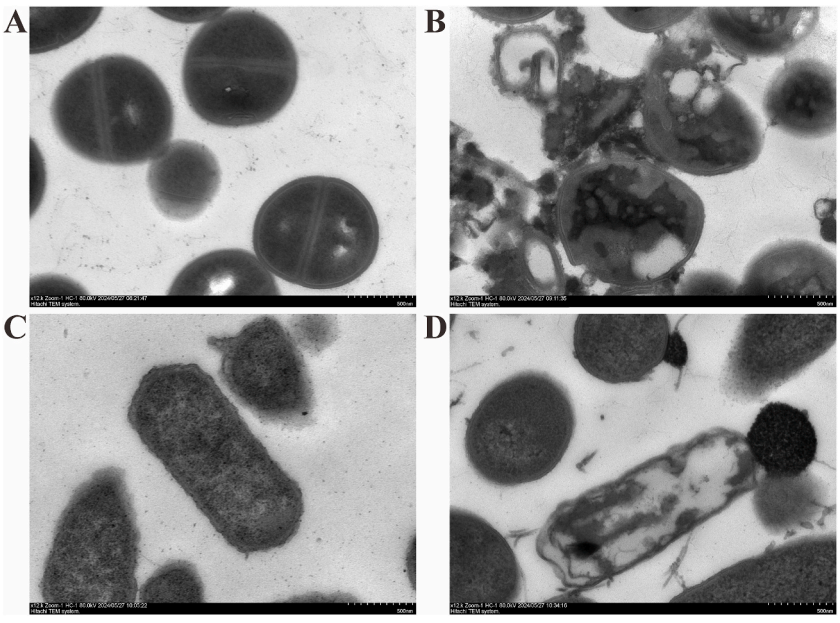

Fig. 7. TEM images of *S. aureus* (A and B), and *E. coli* (C and D) with the treatment of normal saline (A and C as control groups) and N-S/CQDs (B and D as experimental groups).

investigation.

3.8. In vitro cytotoxicity and cell imaging of N-S/CQDs

MTT assay is a colorimetric assay for assessing cell metabolic activity such as cell viability, cytotoxicity, and proliferation. The assay employs a yellow tetrazolium salt, MTT (3-(4,5-dimethylthiazol-2-yl)-2,5-diphenyltetrazolium bromide), which is reduced by metabolically active cells to form an insoluble purple formazan product. This formazan can then be solubilized and quantified by spectrophotometry. In this study, the cytotoxicity of the prepared N-S/CQDs was first assessed *in vitro* using an MTT assay, as shown in Fig. 8. The results demonstrated that even as the concentration of the N-S/CQDs was progressively increased from 32 μg/ml to 1024 μg/ml and the incubation time extended from 24 h to 48 h, the cell survival rate remained impressively high at over 70 %, indicating excellent biocompatibility of the N-S/CQDs. The non-toxicity and high biocompatibility of the N-S/CQDs were highlighted, making them suitable for bioimaging applications. Notably, when the N-S/CQDs were used for cell imaging, the biocompatibility was a critical factor in its effectiveness as fluorescent imaging agents. The implications of these results suggest that the N-S/CQDs, due to its excellent biocompatibility, could serve as superior alternatives to traditional metal-based quantum dots for *in vitro* and *in vivo* imaging applications.

The prepared N-S/CQDs, as applied in cell imaging, exhibited several notable advantages, as evidenced by its performance in staining cells, as illustrated in Fig. 9. In the bright field, the morphology of the test cells was observed to be normal and intact, indicating that the cells maintained their structural integrity during and after exposure to the N-S/CQDs. This is a critical observation as it confirms that the N-S/CQDs are biocompatible and do not adversely affect cell health, which is essential for any material used in biological applications. Transitioning to the dark field, the test cells exhibited a striking blue fluorescence, attributed to the uptake of N-S/CQDs with blue-emitting. The fluorescence was not just a peripheral glow but was evenly distributed throughout the cell, suggesting that the N-S/CQDs were able to permeate the cell membrane and distribute uniformly within the cellular environment. This uniform distribution is beneficial for holistic cellular imaging as it highlights the entire cell structure without bias towards any particular region. Furthermore, the combined images from the bright and dark fields showed a perfect overlap, indicating that the imaging method provided a reliable and accurate representation of the cellular layout. Such clear visualization capability demonstrates the potential of N-S/CQDs in facilitating a deeper understanding of cellular processes and structures, which could be instrumental in areas like cancer research, where understanding cell morphology and behavior is crucial.

The use of N-S/CQDs in cell imaging presents a safer alternative to conventional fluorescent dyes and quantum dots that contain heavy metals, which can be toxic to cells. The biocompatibility and low toxicity of N-S/CQDs underscore their potential for broader applications in medical diagnostics and therapies, enhancing the ability to study cellular processes and disease treatment with minimal adverse effects. For example, it can be used in the treatment of infected wounds to promote wound healing and control local infections [31,68,69].

In addition, the potential of CQDs to revolutionize antibacterial strategies is immense, combining their imaging capabilities with therapeutic functions, which could lead to the development of advanced biocompatible materials for real-time monitoring and treatment of infections. The development and application of CQDs in cell imaging represent a dynamic area of research that combines material science, chemistry, and biotechnology to enhance our understanding and visualization of cellular processes. Future research is likely to focus on enhancing the specificity and efficiency of CQDs in targeting and imaging cells, potentially integrating them with other nanomaterials for multimodal imaging techniques [70].

4. Conclusion

This study focuses on the synthesis of N-S/CQDs utilizing a one-step method with citric acid and cysteine as the primary reaction substrates. The synthesized N-S/CQDs exhibits distinct fluorescence properties, and the fluorescence can be specifically quenched by MnO_4^-. Interestingly, the quenching fluorescence can be effectively recovered by adding GSH, and the recovery intensity increases in proportion to the amount of adding GSH. To leverage this property, a fluorescence sensing system incorporating N-S/CQDs and MnO_4^- was developed and successfully employed to determine GSH content in pharmaceutical preparation. Additionally, the N-S/CQDs demonstrated broad-spectrum antibacterial activity, with MIC of 32 μg/ml against *S. aureus* and 64 μg/ml against *E. coli*. The finding highlight the antibacterial potential of N-S/CQDs. In addition, N-S/CQDs can also be used for cell imaging and has low cytotoxicity, showing excellent biocompatibility.

The multifunctionality and versatile applications of N-S/CQDs, as demonstrated in this study, underscore their significant potential in the fields of biotechnology and nanomedicine. This study not only confirms the promising attributes of N-S/CQDs but also provides a solid foundation for the future development of multifunctional CQDs and their expanded utilization in various domains.

Funding statement

This study was supported by Science and Technology Project of Putian City (2020SP005), Fujian Provincial Natural Science Foundation of China (2023J01160), and Scientific Research Project of Putian University (2022059).

Disclosure statement

No potential conflict of interest was reported by the author(s).

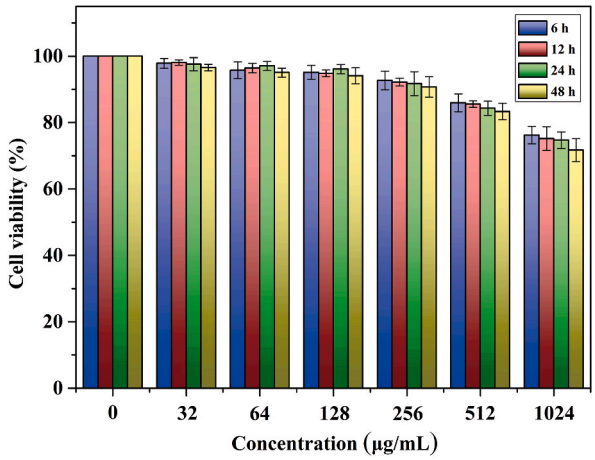

Fig. 8. Cell viability of macrophages treated with different concentrations of N-S/CQDs for 6, 12, 24 and 48 h. Error bars represent the standard deviation of three repeated measurements.

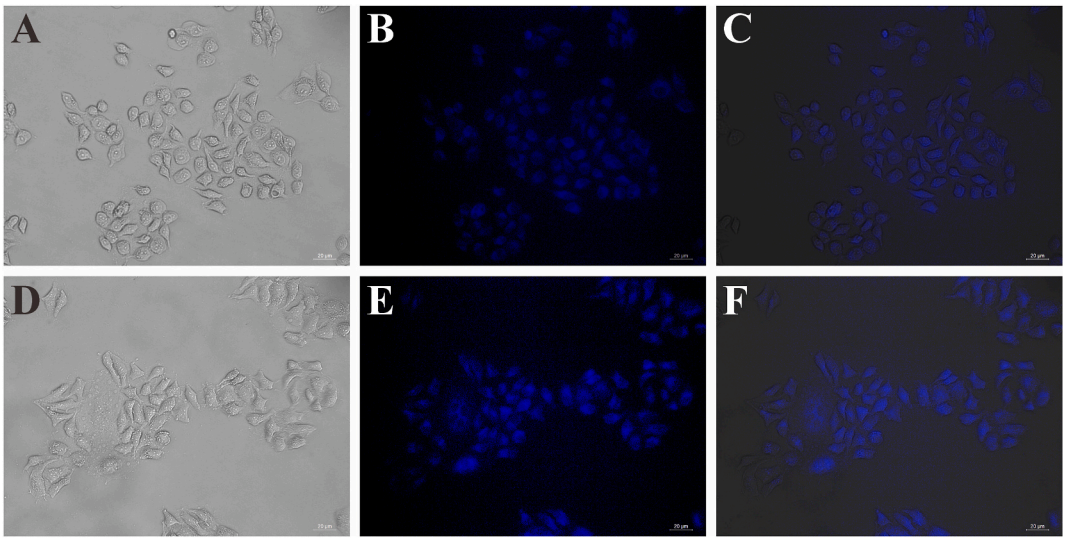

Fig. 9. Fluorescence imaging of N-S/CQDs in macrophages (top row) and HepG2 cells (bottom row).

Data availability statement

The data will be made available upon request.

CRediT authorship contribution statement

Zhipeng Ruan: Writing – review & editing, Writing – original draft, Funding acquisition. **Zhifeng Xu:** Writing – review & editing, Resources, Project administration, Methodology, Formal analysis. **Tianhui Liu:** Writing – review & editing, Data curation, Conceptualization. **Liwen Chen:** Software, Formal analysis, Data curation. **Xiaoling Liu:** Formal analysis, Data curation. **Kaiying Chen:** Supervision, Conceptualization. **Chengfei Zhao:** Writing – review & editing, Supervision, Project administration, Methodology, Data curation, Conceptualization.

Declaration of competing interest

The authors declare that they have no known competing financial interests or personal relationships that could have appeared to influence the work reported in this paper.

References

[1] S.Y. Lim, W. Shen, Z. Gao, Carbon quantum dots and their applications, Chem. Soc. Rev. 44 (2015) 362–381, https://doi.org/10.1039/c4cs00269e.
[2] Y. Dong, R. Wang, H. Li, J. Shao, Y. Chi, X. Lin, G. Chen, Polyamine-functionalized carbon quantum dots for chemical sensing, Carbon 50 (2012) 2810–2815, https://doi.org/10.1016/j.carbon.2012.02.046.
[3] R. Zhang, W. Chen, Nitrogen-doped carbon quantum dots: facile synthesis and application as a "turn-off" fluorescent probe for detection of Hg^{2+} ions, Biosens. Bioelectron. 55 (2014) 83–90, https://doi.org/10.1016/j.bios.2013.11.074.
[4] H. Peng, J. Travas-Sejdic, Simple aqueous solution route to luminescent carbogenic dots from carbohydrates, Chem. Mater. 21 (2009) 5563–5565, https://doi.org/10.1021/cm901593y.
[5] H. Li, X. He, Z. Kang, H. Huang, Y. Liu, J. Liu, S. Lian, C.H. Tsang, X. Yang, S.T. Lee, Water-soluble fluorescent carbon quantum dots and photocatalyst design, Angew Chem. Int. Ed. Engl. 49 (2010) 4430–4434, https://doi.org/10.1002/anie.200906154.
[6] J. Deng, Q. Lu, N. Mi, H. Li, M. Liu, M. Xu, L. Tan, Q. Xie, Y. Zhang, S. Yao, Electrochemical synthesis of carbon nanodots directly from alcohols, Chemistry 20 (2014) 4993–4999, https://doi.org/10.1002/chem.201304869.
[7] S.L. Hu, K.Y. Niu, J. Sun, J. Yang, N.Q. Zhao, X.W. Du, One-step synthesis of fluorescent carbon nanoparticles by laser irradiation, J. Mater. Chem. 19 (2009) 484–488, https://doi.org/10.1039/B812943F.
[8] X. Li, H. Wang, Y. Shimizu, A. Pyatenko, K. Kawaguchi, N. Koshizaki, Preparation of carbon quantum dots with tunable photoluminescence by rapid laser passivation in ordinary organic solvents, Chem. Commun. 47 (2011) 932–934, https://doi.org/10.1039/c0cc03552a.
[9] H. Li, X. He, Y. Liu, H. Huang, S. Lian, S.T. Lee, Z. Kang, One-step ultrasonic synthesis of water-soluble carbon nanoparticles with excellent photoluminescent properties, Carbon 49 (2011) 605–609, https://doi.org/10.1016/j.carbon.2010.10.004.
[10] Y. Liu, N. Xiao, N. Gong, H. Wang, X. Shi, W. Gu, L. Ye, One-step microwave-assisted polyol synthesis of green luminescent carbon dots as optical nanoprobes, Carbon 68 (2014) 258–264, https://doi.org/10.1016/j.carbon.2013.10.086.
[11] S. Sahu, B. Behera, T.K. Maiti, S. Mohapatra, Simple one-step synthesis of highly luminescent carbon dots from orange juice: application as excellent bio-imaging agents, Chem. Commun. 48 (2012) 8835–8837, https://doi.org/10.1039/c2cc33796g.
[12] Y. Yang, J. Cui, M. Zheng, C. Hu, S. Tan, Y. Xiao, Q. Yang, Y. Liu, One-step synthesis of amino-functionalized fluorescent carbon nanoparticles by hydrothermal carbonization of chitosan, Chem. Commun. 48 (2012) 380–382, https://doi.org/10.1039/c1cc15678k.
[13] J.J. Liu, X.L. Zhang, Z.X. Cong, Z.T. Chen, H.H. Yang, G.N. Chen, Glutathione-functionalized graphene quantum dots as selective fluorescent probes for phosphate-containing metabolites, Nanoscale 5 (2013) 1810–1815, https://doi.org/10.1039/c3nr33794d.
[14] Y. Dong, J. Shao, C. Chen, H. Li, R. Wang, Y. Chi, X. Lin, G. Chen, Blue luminescent graphene quantum dots and graphene oxide prepared by tuning the carbonization degree of citric acid, Carbon 50 (2012) 4738–4743, https://doi.org/10.1016/j.carbon.2012.06.002.
[15] Y. Guo, Z. Wang, H. Shao, X. Jiang, Hydrothermal synthesis of highly fluorescent carbon nanoparticles from sodium citrate and their use for the detection of mercury ions, Carbon 52 (2013) 583–589, https://doi.org/10.1016/j.carbon.2012.10.028.
[16] Z.C. Yang, X. Li, J. Wang, Intrinsically fluorescent nitrogen-containing carbon nanoparticles synthesized by a hydrothermal process, Carbon 49 (2011) 5207–5212, https://doi.org/10.1016/j.carbon.2011.07.038.
[17] Q. Liang, W. Ma, Y. Shi, Z. Li, X. Yang, Easy synthesis of highly fluorescent carbon quantum dots from gelatin and their luminescent properties and applications, Carbon 60 (2013) 421–428, https://doi.org/10.1016/j.carbon.2013.04.055.
[18] X. Jia, J. Li, E. Wang, One-pot green synthesis of optically pH-sensitive carbon dots with upconversion luminescence, Nanoscale 4 (2012) 5572–5575, https://doi.org/10.1039/c2nr31319g.
[19] J. Zhou, Z. Sheng, H. Han, M. Zou, C. Li, Facile synthesis of fluorescent carbon dots using watermelon peel as a carbon source, Mater. Lett. 66 (2012) 222–224, https://doi.org/10.1016/j.matlet.2011.08.081.
[20] V.N. Mehta, S. Jha, S.K. Kailasa, One-pot green synthesis of carbon dots by using Saccharum officinarum juice for fluorescent imaging of bacteria (*Escherichia coli*) and yeast (*Saccharomyces cerevisiae*) cells, Mater. Sci. Eng., C 38 (2014) 20–27, https://doi.org/10.1016/j.msec.2014.01.038.
[21] J. Wang, C.F. Wang, S. Chen, Amphiphilic egg-derived carbon dots: rapid plasma fabrication, pyrolysis process, and multicolor printing patterns, Angew Chem. Int. Ed. Engl. 51 (2012) 9297–9301, https://doi.org/10.1002/anie.201204381.
[22] J. Ju, R. Zhang, S. He, W. Chen, Nitrogen-doped graphene quantum dots-based fluorescent probe for the sensitive turn-on detection of glutathione and its cellular imaging, RSC Adv. 4 (2014) 52583–52589, https://doi.org/10.1039/c4ra10601f.
[23] Z. Li, H. Yu, T. Bian, Y. Zhao, C. Zhou, L. Shang, Y. Liu, L.Z. Wu, C.H. Tung, T. Zhang, Highly luminescent nitrogen-doped carbon quantum dots as effective fluorescent probes for mercuric and iodide ions, J. Mater. Chem. C 3 (2015) 1922–1928, https://doi.org/10.1039/c4tc02756f.
[24] J. Ju, W. Chen, Synthesis of highly fluorescent nitrogen-doped graphene quantum dots for sensitive, label-free detection of Fe (III) in aqueous media, Biosens. Bioelectron. 58 (2014) 219–225, https://doi.org/10.1016/j.bios.2014.02.061.
[25] S. Liu, J. Tian, L. Wang, Y. Zhang, X. Qin, Y. Luo, A.M. Asiri, A.O. Al-Youbi, X. Sun, Hydrothermal treatment of grass: a low-cost, green route to nitrogen-doped, carbon-rich, photoluminescent polymer nanodots as an effective fluorescent sensing platform for label-free detection of Cu(II) ions, Adv. Mater. 24 (2012) 2037–2041, https://doi.org/10.1002/adma.201200164.
[26] L. Lin, X. Song, Y. Chen, M. Rong, T. Zhao, Y. Wang, Y. Jiang, X. Chen, Intrinsic peroxidase-like catalytic activity of nitrogen-doped graphene quantum dots and their application in the colorimetric detection of H_2O_2 and glucose, Anal. Chim. Acta 869 (2015) 89–95, https://doi.org/10.1016/j.aca.2015.02.024.
[27] L. Lin, M. Rong, S. Lu, X. Song, Y. Zhong, J. Yan, Y. Wang, X. Chen, A facile synthesis of highly luminescent nitrogen-doped graphene quantum dots for the detection of 2,4,6-trinitrophenol in aqueous solution, Nanoscale 7 (2015) 1872–1878, https://doi.org/10.1039/c4nr06365a.
[28] K.J. Lagos, D. Garcia, C.F. Cuadrado, L.M. de Souza, N.F. Mezzacappo, A.P. da Silva, N. Inada, V. Bagnato, M.P. Romero, Carbon dots: Types, preparation, and their boosted antibacterial activity by photoactivation. Current status and future perspectives, WIRES Nanomed Nanobi 15 (2023) e1887, https://doi.org/10.1002/wnan.1887.
[29] P. Li, X. Yang, X. Zhang, J. Pan, W. Tang, W. Cao, J. Zhou, X. Gong, X. Xing, Surface chemistry-dependent antibacterial and antibiofilm activities of polyamine-functionalized carbon quantum dots, J. Mater. Sci. 55 (2020) 16744–16757, https://doi.org/10.1007/s10853-020-05262-6.
[30] M. Tanaka, M. Kurose, S. Yano, S. Tanaka, N. Gotoh, Y. Nonomura, Structure–activity relationship on selective antibacterial activity of nonionic surfactants, J. Surfactants Deterg. 26 (2023) 789–795, https://doi.org/10.1002/jsde.12704.
[31] Y. Wu, C. Li, H.C. van der Mei, H.J. Busscher, Y. Ren, Carbon quantum dots derived from different carbon sources for antibacterial applications, Antibiotics (Basel) 10 (2021) 623, https://doi.org/10.3390/antibiotics10060623.
[32] K.M. Tripathi, H.T. Ahn, M. Chung, X.A. Le, D. Saini, A. Bhati, S.K. Sonkar, M.I. Kim, T. Kim, N, S, and P-co-doped carbon quantum dots: intrinsic peroxidase activity in a wide ph range and its antibacterial applications, ACS Biomater. Sci. Eng. 6 (2020) 5527–5537, https://doi.org/10.1021/acsbiomaterials.0c00831.
[33] N. Tejwan, A.K. Saini, A. Sharma, T.A. Singh, N. Kumar, J. Das, Metal-doped and hybrid carbon dots: a comprehensive review on their synthesis and biomedical applications, J. Contr. Release 330 (2021) 132–150, https://doi.org/10.1016/j.jconrel.2020.12.023.
[34] A. Saravanan, P. Das, M. Maruthapandi, S. Aryal, S. Michaeli, Y. Mastai, J.H. Luong, A. Gedanken, Heteroatom co-doping (N, NS, NB) on carbon dots and their antibacterial and antioxidant properties, Surface. Interfac. 46 (2024) 103857, https://doi.org/10.1016/j.surfin.2024.103857.
[35] J.A. Jaleel, K. Pramod, Artful and multifaceted applications of carbon dot in biomedicine, J. Contr. Release 269 (2018) 302–321, https://doi.org/10.1016/j.jconrel.2017.11.027.
[36] M. Liu, Y. Xu, F. Niu, J.J. Gooding, J. Liu, Carbon quantum dots directly generated from electrochemical oxidation of graphite electrodes in alkaline alcohols and the applications for specific ferric ion detection and cell imaging, Analyst 141 (2016) 2657–2664, https://doi.org/10.1039/c5an02231b.
[37] Z. Fatahi, N. Esfandiari, H. Ehtesabi, Z. Bagheri, H. Tavana, Z. Ranjbar, H. Latifi, Physicochemical and cytotoxicity analysis of green synthesis carbon dots for cell imaging, EXCLI J 18 (2019) 454–466, https://doi.org/10.17179/excli2019-1465.
[38] K.J. Mintz, Y. Zhou, R.M. Leblanc, Recent development of carbon quantum dots regarding their optical properties, photoluminescence mechanism, and core structure, Nanoscale 11 (2019) 4634–4652, https://doi.org/10.1039/c8nr10059d.

[39] S.K. Kailasa, S. Ha, S.H. Baek, L.M.T. Phan, S. Kim, K. Kwak, T.J. Park, Tuning of carbon dots emission color for sensing of Fe^{3+} ion and bioimaging applications, Mater. Sci. Eng., C 98 (2019) 834–842, https://doi.org/10.1016/j.msec.2019.01.002.

[40] N. Devi, N. Wangoo, Tuning the luminescence of microwave-assisted n-doped fluorescent carbon dots: bioimaging applications and label-free anti-cancer drug delivery, ACS Appl. Bio Mater. 6 (2023) 999–1010, https://doi.org/10.1021/acsabm.2c00850.

[41] L. Ansari, S. Hallaj, T. Hallaj, M. Amjadi, Doped-carbon dots: recent advances in their biosensing, bioimaging and therapy applications, Colloids Surf. B Biointerfaces 203 (2021) 111743, https://doi.org/10.1016/j.colsurfb.2021.111743.

[42] W. Yang, H. Zhang, J. Lai, X. Peng, Y. Hu, W. Gu, L. Ye, Carbon dots with red-shifted photoluminescence by fluorine doping for optical bio-imaging, Carbon 128 (2018) 78–85, https://doi.org/10.1016/j.carbon.2017.11.069.

[43] P. Lesani, G. Singh, C.M. Viray, Y. Ramaswamy, M. Zhu, P. Kingshott, Z. Lu, H. Zreiqat, Two-photon dual-emissive carbon dot-based probe: deep-tissue imaging and ultrasensitive sensing of intracellular ferric ions, ACS Appl. Mater. Interfaces 12 (2020) 18395–18406, https://doi.org/10.1021/acsami.0c05217.

[44] Z. Liu, J. Xiao, X. Wu, L. Lin, S. Weng, M. Chen, X. Cai, X. Lin, Switch-on fluorescent strategy based on N and S co-doped graphene quantum dots (NS/GQDs) for monitoring pyrophosphate ions in synovial fluid of arthritis patients, Sensor Actuat B-Chem 229 (2016) 217–224, https://doi.org/10.1016/j.snb.2016.01.127.

[45] C. Zhao, K. Wang, Q. Cai, H. Tu, L. Pan, L. Yu, Signal-on fluorescent sensor based on N-CQDs for the detection of glutathione in human serum and pharmaceutic preparation, Prep. Biochem. Biotechnol. 47 (2017) 835–840, https://doi.org/10.1080/10826068.2017.1342267.

[46] C. Zhao, X. Wang, L. Yu, L. Wu, X. Hao, Q. Liu, L. Lin, Z. Huang, Z. Ruan, S. Weng, A. Liu, X. Lin, Quaternized carbon quantum dots with broad-spectrum antibacterial activity for the treatment of wounds infected with mixed bacteria, Acta Biomater. 138 (2022) 528–544, https://doi.org/10.1016/j.actbio.2021.11.010.

[47] P. Namdari, B. Negahdari, A. Eatemadi, Synthesis, properties and biomedical applications of carbon-based quantum dots: an updated review, Biomed. Pharmacother. 87 (2017) 209–222, https://doi.org/10.1016/j.biopha.2016.12.108.

[48] A. Vibhute, T. Patil, R. Gambhir, A.P. Tiwari, Fluorescent carbon quantum dots: synthesis methods, functionalization and biomedical applications, Applied Surface Science Advances 11 (2022) 100311, https://doi.org/10.1016/j.apsadv.2022.100311.

[49] F. Zu, F. Yan, Z. Bai, J. Xu, Y. Wang, Y. Huang, X. Zhou, The quenching of the fluorescence of carbon dots: a review on mechanisms and applications, Microchim. Acta 184 (2017) 1899–1914, https://doi.org/10.1007/s00604-017-2318-9.

[50] Y. Song, S. Zhu, S. Xiang, X. Zhao, J. Zhang, H. Zhang, Y. Fu, B. Yang, Investigation into the fluorescence quenching behaviors and applications of carbon dots, Nanoscale 6 (2014) 4676–4682, https://doi.org/10.1039/c4nr00029c.

[51] L. Bao, Z.L. Zhang, Z.Q. Tian, L. Zhang, C. Liu, Y. Lin, B. Qi, D.W. Pang, Electrochemical tuning of luminescent carbon nanodots: from preparation to luminescence mechanism, Adv. Mater. 23 (2011) 5801–5806, https://doi.org/10.1002/adma.201102866.

[52] H. Shi, Q. Zhao, C.-H. Zhou, N.-Q. Jia, Nitrogen and sulfur co-doped carbon quantum dots as fluorescence sensor for detection of lead ion, Chin. J. Anal. Chem. 50 (2022) 63–68, https://doi.org/10.1016/j.cjac.2021.09.010.

[53] G. Wang, S. Zhang, J. Cui, W. Gao, X. Rong, Y. Lu, C. Gao, Preparation of nitrogen-doped carbon quantum dots from chelating agent and used as fluorescent probes for accurate detection of ClO^- and Cr(VI), Anal. Chim. Acta 1195 (2022) 339478, https://doi.org/10.1016/j.aca.2022.339478.

[54] S.M. Abd Elhaleem, F. Elsebaei, S. Shalan, F. Belal, Turn-off fluorescence of nitrogen and sulfur carbon quantum dots as effective fluorescent probes for determination of imatinib. Application to biological fluids, Spectrochim. Acta Mol. Biomol. Spectrosc. 272 (2022) 120954, https://doi.org/10.1016/j.saa.2022.120954.

[55] Y. Yang, T. Zou, Z. Wang, X. Xing, S. Peng, R. Zhao, X. Zhang, Y. Wang, The fluorescent quenching mechanism of N and S co-doped graphene quantum dots with Fe^{3+} and Hg^{2+} Ions and their application as a novel fluorescent sensor, Nanomaterials 9 (2019) 738, https://doi.org/10.3390/nano9050738.

[56] Y.J. Tu, Y.H. Tian, Y.L. Yang, High-sensitivity and selectivity detection of permanganate ions based on pig liver-based carbon quantum dots, Appl. Ecol. Environ. Res. 17 (2019) 7249–7263, https://doi.org/10.15666/aeer/1704_72497263.

[57] S. Zhu, Q. Meng, L. Wang, J. Zhang, Y. Song, H. Jin, K. Zhang, H. Sun, H. Wang, B. Yang, Highly photoluminescent carbon dots for multicolor patterning, sensors, and bioimaging, Angew Chem. Int. Ed. Engl. 52 (2013) 3953–3957, https://doi.org/10.1002/anie.201300519.

[58] T.H. Le, J.H. Kim, S.J. Park, "Turn on" fluorescence sensor of glutathione based on inner filter effect of co-doped carbon dot/gold nanoparticle composites, Int. J. Mol. Sci. 23 (2021) 190, https://doi.org/10.3390/ijms23010190.

[59] Q. Ma, M. Wang, H. Cai, F. Li, S. Fu, Y. Liu, Y. Zhao, A sensitive and rapid detection of glutathione based on a fluorescence-enhanced "turn-on" strategy, J. Mater. Chem. B 9 (2021) 3563–3572, https://doi.org/10.1039/d1tb00232e.

[60] M.I. Halawa, F. Wu, M.N. Zafar, I.M. Mostafa, A. Abdussalam, S. Han, G. Xu, Turn-on fluorescent glutathione detection based on lucigenin and MnO_2 nanosheets, J. Mater. Chem. B 8 (2020) 3542–3549, https://doi.org/10.1039/c9tb02158b.

[61] H.B. Wang, Y. Chen, Y. Li, Y.M. Liu, A sensitive fluorescence sensor for glutathione detection based on MnO_2 nanosheets–copper nanoclusters composites, RSC Adv. 6 (2016) 79526–79532, https://doi.org/10.1039/c6ra17850b.

[62] P. Zhao, B. Jin, Q. Zhang, R. Peng, High-quality carbon nitride quantum dots on photoluminescence: effect of carbon sources, Langmuir 37 (2021) 1760–1767, https://doi.org/10.1021/acs.langmuir.0c02966.

[63] P. Li, S. Liu, W. Cao, G. Zhang, X. Yang, X. Gong, X. Xing, Low-toxicity carbon quantum dots derived from gentamicin sulfate to combat antibiotic resistance and eradicate mature biofilms, Chem. Commun. 56 (2020) 2316–2319, https://doi.org/10.1039/c9cc09223d.

[64] R. Zhao, M. Lv, Y. Li, M. Sun, W. Kong, L. Wang, S. Song, C. Fan, L. Jia, S. Qiu, Y. Sun, H. Song, R. Hao, Stable nanocomposite based on pegylated and silver nanoparticles loaded graphene oxide for long-term antibacterial activity, ACS Appl. Mater. Interfaces 9 (2017) 15328–15341, https://doi.org/10.1021/acsami.7b03987.

[65] X. Hao, L. Huang, C. Zhao, S. Chen, W. Lin, Y. Lin, L. Zhang, A. Sun, C. Miao, X. Lin, M. Chen, S. Weng, Antibacterial activity of positively charged carbon quantum dots without detectable resistance for wound healing with mixed bacteria infection, Mater. Sci. Eng., C 123 (2021) 111971, https://doi.org/10.1016/j.msec.2021.111971.

[66] A. Vibhute, O. Nille, G. Kolekar, S. Rohiwal, S. Patil, S. Lee, A.P. Tiwari, Fluorescent carbon quantum dots functionalized by poly L-Lysine: efficient material for antibacterial, bioimaging and antiangiogenesis applications, J. Fluoresc. 32 (2022) 1789–1800, https://doi.org/10.1007/s10895-022-02977-4.

[67] Z. Wang, J. Zhu, L. Chen, K. Deng, H. Huang, Multifunctional gold-silver-carbon quantum dots nano-hybrid composite: advancing antibacterial wound healing and cell proliferation, ACS Appl. Mater. Interfaces 15 (2023) 40241–40254, https://doi.org/10.1021/acsami.3c07625.

[68] A. Salleh, M.B. Fauzi, The in Vivo, in vitro and in ovo evaluation of quantum dots in wound healing: a review, Polymers 13 (2021) 191, https://doi.org/10.3390/polym13020191.

[69] S.H. Hamed, E.A. Azooz, E.A.J. Al-Mulla, Nanoparticles-assisted wound healing: a review, Nano Biomed Eng 15 (2023) 425–435, https://doi.org/10.26599/NBE.2023.9290039.

[70] X. Han, C. Zhao, S. Wang, Z. Pan, Z. Jiang, X. Tang, Multifunctional TiO_2/C nanosheets derived from 3D metal-organic frameworks for mild-temperature-photothermal-sonodynamic-chemodynamic therapy under photoacoustic image guidance, J. Colloid Interface Sci. 621 (2022) 360–373, https://doi.org/10.1016/j.jcis.2022.04.077.